International Journal of Biological Macromolecules 275 (2024) 133722

Contents lists available at ScienceDirect

International Journal of Biological Macromolecules

journal homepage: www.elsevier.com/locate/ijbiomac

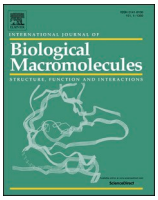

The dark side of the wool? From wool wastes to keratin microfilaments through the solution blow spinning process

Giorgia Maurizii [a], Laura Valentini [a], Giovanna Sotgiu [b,c], Roberto Zamboni [b,c], Cinzia Tonetti [d], Claudia Vineis [d], Barbara Canonico [a], Mariele Montanari [a], Mattia Tiboni [a], Luca Casettari [a], Annalisa Aluigi [a,c,*]

[a] Department of Biomolecular Sciences, University of Urbino Carlo Bo, Piazza del Rinascimento, 6, 61029 Urbino (PU), Italy
[b] Institute of Organic Synthesis and Photoreactivity – Italian National Research Council, Via P. Gobetti, 101, Bologna, 40129, Italy
[c] Kerline srl, Via Piero Gobetti 101, Bologna, 40129, Italy
[d] CNR-STIIMA (National Research Council—Institute of Intelligent Industrial Technologies and Systems for Advanced Manufacturing), Corso Giuseppe Pella 16, 13900, Biella, Italy

ARTICLE INFO

Keywords:
Keratin
Solution blow spinning
Tissue engineering

ABSTRACT

The valorization of discarded wool from dairy sheep breeding is a challenging issue. The most proposed strategies lie in the processing of keratin extracted from wool without reducing the molecular weight of the protein chains (the high molecular weight-HMW keratin). Here, the HMW keratin has been spun for the first time by solution blow spinning. A screening study of the process carried out with a 2-level full factorial design revealed that keratin filaments can be obtained by using the polyethylene oxide at 900 kDa, a 2 bar air pressure, and a 30 cm needle-collector distance. An annealing at 80 °C for 15 min, at pH 3.5 with citric acid contributes to increasing the viscosity of the keratin solutions thereby allowing the production of defect-free and water-stable filaments having diameters from 1 to 6 μm. A negligible toxic effect was observed after 24 and 48 h on HT29 epithelial cells and normal blood cells displayed behavior similar to the control demonstrating that the patches are hemocompatible. Therefore, the developed SBS process of keratin aqueous solutions could represent a valuable platform for developing patches that need to be blood-contacting and deposited in-situ.

1. Introduction

Wool wastes deriving from sheep breeding for the dairy industries and slaughterhouses are poor quality fibers not suitable for textile purposes [1]. The annual production of these wool wastes amounts to >200 thousand tonnes in Europe alone, and, if not used, they are classified as special wastes to be disposed of [2]. A very small part of these wastes is used to produce fertilizers and feed; however, the majority is landfilled or incinerated, even if these are processes with a high environmental impact. Alternative management routes have been proposed to reduce their accumulation in the environment. Their valorization mainly consists of biorefinery processes aimed at extracting valuable keratin for added-value applications [3].

This wool contains up to 95 % by weight of pure keratin with molecular weights ranging from 45 to 60 kDa and 11–28 kDa [4], which have peculiar properties such as biodegradability, biocompatibility, bioactivity (i.e. the ability to promote cell growth), ability to bind toxic substances (i.e. heavy metals and formaldehyde) and to vehiculate both hydrophilic and lipophilic active ingredients. For this reason, the scientific literature is full of works proposing different keratin-based materials for textile applications [5], for the purification of air and water [6], for the controlled delivery of active ingredients [7] and for the regeneration of biological tissues [8,9]. Although keratin has been transformed into various structured materials such as films, sponges, and/or hydrogels, their spinning into filaments is still a very challenging process to be faced [10] [11].

The development of filaments with a high keratin content is of particular interest both for re-ennobling raw wool in the textile sector [11] and for realizing protein scaffolds mimicking the cellular matrix (ECM) able to promote biological tissue reconstruction and skin regeneration at injury sites [12] [13]. Among the spinning processes for wool keratin, electrospinning (ES) and wet spinning (WS) are certainly the

* Corresponding author at: Department of Biomolecular Sciences, University of Urbino Carlo Bo, Piazza del Rinascimento, 6, Urbino (PU) 61029, Italy.
E-mail address: annalisa.aluigi@uniurb.it (A. Aluigi).

https://doi.org/10.1016/j.ijbiomac.2024.133722
Received 30 January 2024; Received in revised form 19 June 2024; Accepted 5 July 2024
Available online 6 July 2024

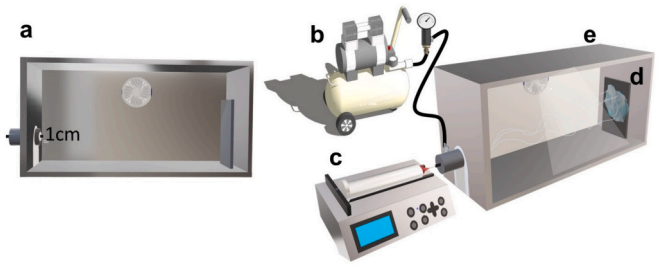

Fig. 1. Schematic representation of the home-made solution blow spinning set-up: a) co-axial spinneret hosting the syringe metal needle in the inner channel, and pressured air in the outer channel, b) air compressor, c) syringe pump, d) collector, and e) heated chamber.

Table 1
Input parameters and observed responses in a 2-level full factorial design.

Run	X_1 PEO molecular weight (MW) – KDa	X_2 Air pressure Bar	X_3 Solution feed rate mL/min	X_4 Needle-collector distance cm	Y Morphology Score**
1	100	5	0.05	30	1
2	900	5	0.05	30	4
3	900	2	0.05	15	5
4	100	2	0.05	15	2
5	900	5	0.2	30	3
6	100	5	0.2	30	1
7	900	5	0.2	15	2
8	100	5	0.05	15	1
9	100	5	0.2	15	1
10	100	2	0.2	30	2
11	900	5	0.05	15	2
12	100	2	0.05	30	2
13	900	2	0.2	30	5
14	900	2	0.2	15	4
15	100	2	0.2	15	1
16	900	2	0.05	30	5
1	100	5	0.05	30	1

** Score: 1 - no fiber and wet sample; 2 - no fiber, dry sample; 3 - no fiber, dry and free-standing sample; 4 - fiber but not free-standing sample and 5 - fiber and free standing sample.

most studied processes. Instead, to the best of our knowledge, there are no works relating to the solution blow spinning (SBS) process of wool keratin or that coming from any other source (e.g. feathers, hair, etc.).

In the SBS process, a polymeric fluid in the form of a solution or a suspension is pumped through the internal channel of a coaxial needle having a small diameter. Highly pressurized air is made to flow along the external channel, thus favouring the expulsion of the polymeric jet towards a collector placed at a certain distance in front of the nozzle, the stretching of the polymeric chains, and the evaporation of the solvent [14]. With the SBS process, the control of fiber dimension and morphology is more difficult than with other spinning technologies. Nevertheless, the main advantage of SBS over the other spinning technologies is the possibility of a safe in situ deposition of the fibrous materials, on any kind of surface. The high potential of the SBS technology for the in-situ deposition was highlighted by Gao et al., who proposed a laparoscopic hemostasis surgery to treat a pig liver wound, by using a portable SBS device [16]. Even if recently advances in portable electrospinning apparatus, for the in situ delivery of personalized wound care have been reported [15], the use of high-voltage systems in these devices could still represent a risk, especially for laparoscopic applications.

Although a myriad of polymers has been processed by SBS, for in situ deposition onto a biological tissue, safety considerations regarding the solvent choice are needed. Most solvents suitable for the SBS process are too toxic and have the potential to cause harm to be considered for in-situ applications. On the other hand, spinning from non-toxic solvents such as water is challenging. Indeed, due to the relatively low volatility of water, drying the fibers before reaching the collector is difficult and this involves the loss of the fibrous architecture in the final material.

In the present work, the solution blow spinning process of wool keratin was pioneeringly considered. To develop a process suitable for the in situ spinning of the patch, only water was considered as a solvent for keratin solutions to be processed. A screening of the process parameters that mainly influence the morphology of the spun samples was carried out through the Design of Experiment (DoE) approach implemented with a 2-level full factorial design [17].

Afterward, the crosslinking process of keratin fibers using citric acid has been optimized by studying the relationship between the crosslinking conditions (in terms of citric acid amount, reaction temperature and pH) and viscosity of the spinning solutions, as well as stability and morphology of the spun patches. The crosslinking mechanism was investigated by FTIR measurements.

To validate the keratin spun patches as materials for biomedical applications, their interactions with HT29 epithelial cells as well as their hemocompatibility were evaluated by Flow Cytometry optical and confocal microscopic analysis. The HT29 cells have been selected as model cell lines already indicated by several research groups for biocompatibility tests of materials addressed to the wound healing of intestinal epithelium [18–20].

2. Materials and methods

2.1. Materials

PEO at a molecular weight of 100 kDa (PEO100) was purchased from Sigma-Aldrich; while PEO with a molecular weight of 900 kDa (PEO900) was kindly supplied by DuPont. All other chemicals were purchased by Thermo Fischer Scientific.

2.2. Extraction of keratin from wool

The high molecular weight keratin (HMW keratin 45–55 kDa) was extracted from coarse wool using an industrial process that can not be detailed for the sake of industrial secrecy.

Briefly, degreased and cleaned wool fibers collected by several local farmers were treated with aqueous solutions containing urea and sodium sulfite. After the wool dissolution, the HMW keratin was purified through multi-step filtration with decreasing cut-off, followed by dialysis against distilled water. The molecular weights distribution of keratin is shown in **Fig. S1.**

2.3. Experimental Design of the SBS Process

Keratin was dissolved in water at a concentration of 10 % *w/V*, under stirring for 2 h. Then, two different solutions were prepared: one with PEO100 and the other with PEO900. The PEO was added at a concentration of 2 % w/V and the mixture was maintained under stirring overnight.

For the SBS processing, a 3D-printed device schematized in Fig. 1 was employed [21]. Briefly, the device consists of a coaxial spinneret hosting a metal needle of a syringe in the inner channel, while pressured air is flown in the outer channel (Fig. 1a), an air compressor (Fig. 1b), a syringe pump to control the flow of the polymer solution (Fig. 1c), and a collector (Fig. 1d) inside a heated chamber (Fig. 1e). The protrusion of the syringe needle at the nozzle exit was set to 1 cm (Fig. 1a), and the needle was inserted directly into the heated chamber where the polymer solution was ejected towards the collector. The temperature inside the chamber was maintained between 30 °C and 40 °C to promote the solvent evaporation.

The solutions were processed into filaments by varying the air

Table 2
ANOVA parameters and validation of the Design Space.

Source	p-value		Source	p-value	
Complete model	0,0054	significant	**Reduced model**	< 0.0001	Significant
X_1 - PEO (MW)	0,0002		X_1 - PEO (MW)	< 0.0001	Significant
X_2 - Air pressure	0,0030		X_2 - Air pressure	0,0002	Significant
X_3 – Flux	0,2031	Not significant	X_4 -Distance	0,0280	Significant
X_4 -Distance	0,0587		X_1X_2	0,0280	Significant
X_1X_2	0,0587				
X_1X_3	0,6462	Not significant			
X_1X_4	0,2031	Not significant			
X_2X_3	0,6462	Not significant			
X_2X_4	0,6462	Not significant			
X_3X_4	0,6462	Not significant			
Complete model - Fit Statistics			**Reduced model - Fit Statistics**		
R^2	0,9635		**R^2**	0,9252	
Adjusted-R^2	0,8904		**Adjusted-R^2**	0,8980	
Predicted-R^2	0,6260		**Predicted-R^2**	0,8418	

pressure, the flow rate, and the distance between the needle and the collector (see Video 1). The influence of the PEO molecular weight (X_1), air pressure (X_2), flow rate (X_3) and needle-collector distance (X_4) on the morphology of the spun samples was evaluated by means of a 2-level full factorial design (2^4), where two levels for each factor were defined (as shown in Table S1). The design required 16 experiments (runs) listed in Table 1. The evaluation of the morphology was carried out by attributing a coded score from 1 to 5 as described below: 1 - no fiber and wet sample; 2 - no fiber, dry sample; 3 - no fiber, dry and free-standing sample; 4 - fiber but not free-standing sample and 5 - fiber and free-standing sample.

The analysis of variance (ANOVA) was performed to evaluate the effects of main input factors (X_1, X_2, X_3, X_4) and the related 2-factor interactions with them ($X_1X_2, X_1X_3, X_1X_4, X_2X_3, X_2X_4, X_3X_4$), as shown in Table 2. A statistically significant level of 5 % was considered and regression coefficients R^2, adjusted-R^2 (adj-R^2), and predicted R^2 (pred-R^2) were used to validate the mathematical model correlating the input factors with the samples' morphology (output value). The data were analyzed by using MATLAB and ORIGIN PRO 2021 software.

2.4. Crosslinking

Aqueous solutions of citric acid (10 % wt) were prepared at pH 3.5 and 7. The pH was adjusted by adding the desired amount of sodium hydroxide (5 M). Keratin was dissolved in water and a desired amount of the citric acid solution was added. The concentration of keratin in the final solution was 10 % *w/V*. Citric acid was added at a concentration of 10 % and 20 % to keratin weight, and a pH of both 3.5 and 7. The prepared solutions were maintained under shaking for 2 h. After that, the PEO900 at a concentration of 2 % w/V was added and its dissolution was performed under shaking, overnight. The resulting solutions were then annealed at 80 °C in a water bath for 15 min. Then the solutions were processed by SBS using the optimized conditions of 2 bar air pressure, 0.125 mL/min solutions feed rate, and 30 cm of needle-collector distance. A part of the obtained fibers was heated at 150 °C, using a hot plate for 5 min.

2.5. Characterization

2.5.1. Rheological characterization

The solutions were characterized with a rotational rheometer (RheolabQC Anton Paar), using a concentric cylinder measuring system, in the share-rate range of 1–1000 s^{-1}, at a temperature of 25 °C. The rheological characterization was carried out on pre-annealed solutions, as well as on the annealed solutions. The keratin/PEO solution without citric acid was considered as a reference.

2.5.2. Scanning Electron Microscopy (SEM)

The morphology of spun samples prepared during the screening phase was investigated by using an EVO10 Scanning Electron Microscope (SEM, Carl Zeiss Microscopy GmbH) with an acceleration voltage of 20 kV. The samples were sputter-coated with a 20 nm-thick gold layer in rarefied argon (20 Pa), using a Quorum SC7620 Sputter Coater.

For the measurement of the fiber diameters of each sample, 100 fibers randomly collected from different SEM images were analyzed by using the GIMP 2.8 (GNU Image Manipulation Program) software.

2.5.3. Stability test

To evaluate the crosslinking, all the obtained fibers (approximatively 1.5 mg), previously dried at 50 °C for 2 h, were immersed in 5 mL of deionized water at 37 °C for 24 h. After that, the samples were centrifuged and the precipitate was recovered and dried at 50 °C, overnight. The stability was evaluated using the eq. 1 (Eq.1):

$$\%Stability = \frac{Measured\ amount\ of\ insolubilized\ sample\ (g)}{Amount\ of\ initial\ sample\ (g)} \times 100 \quad (1)$$

2.5.4. Infrared spectroscopy

Investigation on crosslinking mechanism was performed using attenuated total FTIR (ATR-FTIR, Spectrum Two FT-IR spectrometer with ATR accessory, Perkin Elmer, MA, USA), in the wavenumbers range of 500–4000 cm^{-1}, with a resolution of 2 cm^{-1} and using 32 scans.

2.5.5. Texture analyzer

Track measurements were performed using a texture analyzer (TA. XTPlus, Stable Micro Systems, Godalming, UK) both on untreated and thermally stabilized (150 °C) keratin spun patches. The specimens were placed on the working stage of the instrument and a cylindrical stainless-steel probe, coupled with a 5-kg load cell, was lowered down at a rate of 1 mm/s to press on the sample with a force of 5 N. Then the probe was removed at a rate of 0.5 mm/s while the force was recorded. Six replicate analyses were performed at room temperature using a fresh sample in each case. Force–distance curves were recorded and maximal force, AUC, and elongation at detachment were evaluated using Origin Software.

2.5.6. Establishing a preliminary protocol to evaluate patch/cell interactions

The spun samples were washed with cell medium (RPMI 1640) using the following procedure: the patch (about 5 mm length vs width) was placed in a volume of 1 mL of RPMI for about 2 h, then mild centrifugation (1500 rpm × 10 min) was performed to discard the supernatant and collect the keratin samples. The patch, soaked and with a gelatinous appearance, has been recovered and added to the HT29 epithelial intestinal tumor cell line, seeded at 2×10^5 of cell in a six-well plate.

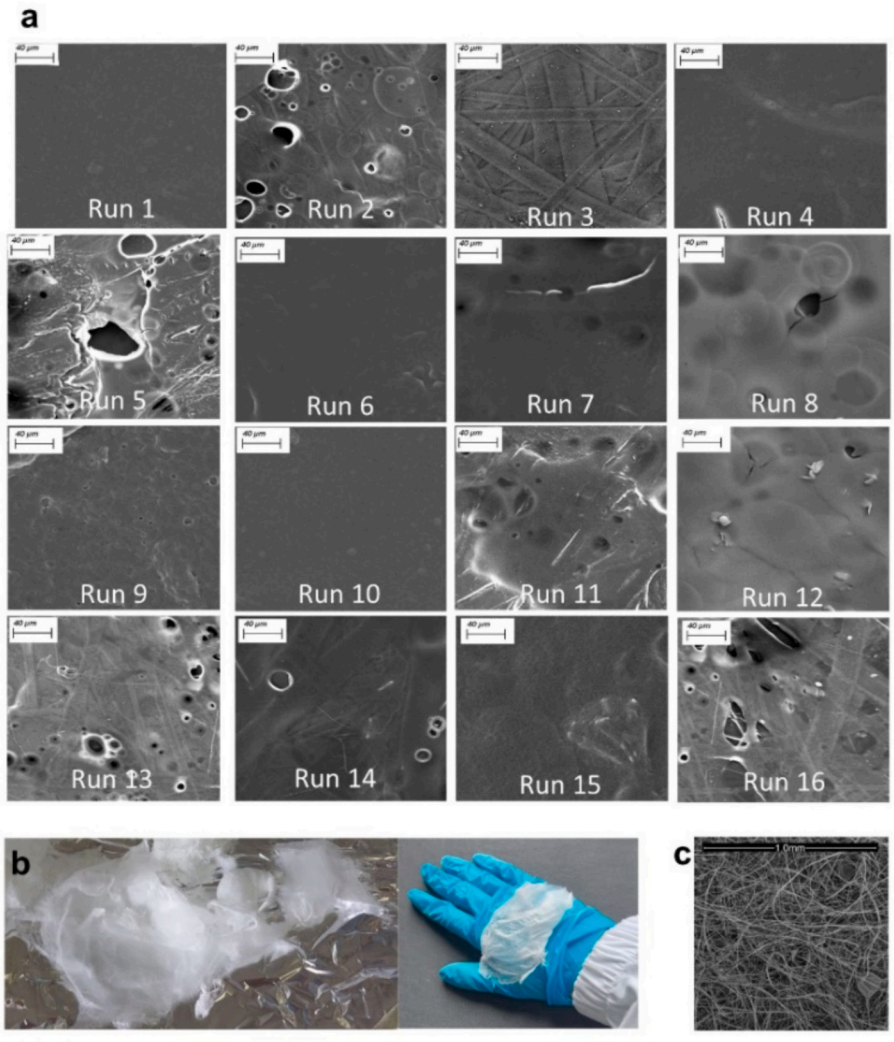

Fig. 2. a) Scanning electron micrographs of the samples obtained via solution blow spinning of keratin-based solutions by applying the spinning conditions of the runs listed in Table 1. b) Visual appearance and c) SEM images of the spun patches obtained by using the PEO 900 kDa at a concentration of 2%wt, an air pressure of 2 bar, a needle-collector distance of 30 cm and solution feed rate of 0.125 mL/min.

Supernatants were collected and the cell layer was trypsinized for 3–4 min, then, after trypsin inactivation by FBS, cells were harvested and washed at 300 g. Pre-collected supernatants were added to the cellular pellets to restore the treatment conditions of the plate wells as much as possible. To avoid technical problems during cytometric acquisition, samples were filtered by 30 μm mesh, to discard the largest/longest fibers (to avoid instrumentation damages). Conversely, for Confocal Microscopy analyses, filtration was not applied, to appreciate contacts between cells and fibers. All qualitative and quantitative tests were conducted after 24 and 48 h.

2.5.7. Establishing a brief preliminary test to evaluate patch hemocompatibility

Although hemocompatibility is particularly evaluated for blood-contacting biomaterials and extensive in vitro analyses according to ISO 10993-4 are required before clinical application [22], we performed a hemocompatibility test on the keratin patches. In these prospects, we proceeded into consideration some main parameters of the blood cell components The quality of collected blood enables standardized hemocompatibility in vitro analysis: fresh blood from healthy subjects [23] was used within 4 h after the blood collection.

2.5.8. Static system

We employed the simplest testing option which is the static model: blood was incubated with the patch in a test tube without a continuous mixing. This test has the advantages of simplicity, speed, and the possibility of testing a large number of samples at once, as reported [24]. The experimental protocol was performed according to the Helsinki Declaration of 1975 as revised in 2008 regarding ethical principles for medical research involving human subjects. No specific Ethical approval was required: blood was obtained from healthy volunteers included in the Italian blood donor registry [registered Associazione Volontari Italiani del Sangue (AVIS) donors] and was provided by the *S. Maria* della Misericordia Hospital in Urbino. A formal agreement exists between the Hospital of Urbino and the Department of Biomolecular Sciences (DISB) for the use of blood and its product for laboratory application and research in producing in vitro medical diagnostic devices.

2.5.9. Flow cytometry on cell lines and blood cell components

Cell viability was assessed using 7-AAD staining [25]. The cells were incubated for 10 min in the dark with 7-AAD (Beckman Coulter, USA). We detected 7AAD-positive events, indicating the percentage of dead cells Mitochondrial functions were investigated through Tetra-methyl rhodamine ethyl ester perchlorate (TMRE) staining [26]. TMRE

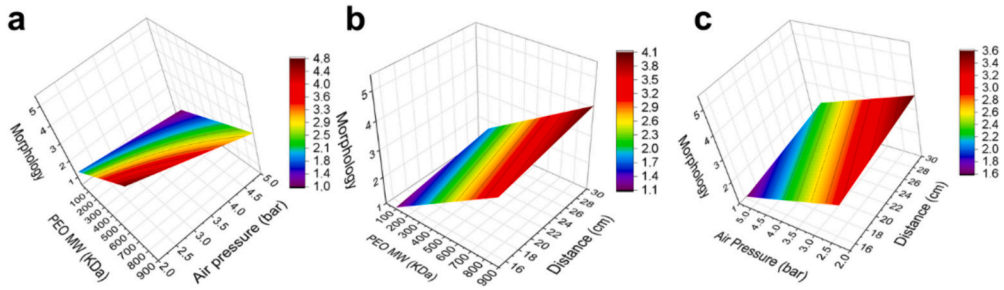

Fig. 3. Design space for morphology as a function of PEO MW, air pressure, and distance.

(Sigma-Aldrich) is a cationic dye that penetrates the mitochondria and generates a red–orange fluorescence as intense as the mitochondrial membrane potential. TMRE 40 nM was added to the sample 15 min before the acquisition time. LysoTracker Green (LTG) dye (Thermo Fisher Scientific, USA) was used to evaluate the lysosome network [27]. Briefly, LysoTracker is an acid-tropic fluorescent probe useful for the monitoring of acid organelles in living cells. The amount of fluorescence obtained by LysoTracker staining is directly proportional to the volume of lysosomes in the cell. LysoTracker 100 nM was evaluated after 30 min of incubation with cells and a green lysosomal fluorescence was collected. The samples were analyzed by a FACSCanto II (BD) flow cytometer equipped with an argon laser (Blue, Ex 488 nm), a helium neon laser (Red, Ex 633 nm), and a solid-state diode laser (Violet, Ex 405 nm). The analyses were performed with the FACSDiva™ (BD) software. At least 10,000 cellular events were acquired for each sample.

Indeed, the following mAbs: anti CD42b FITC conjugated (clone HIP1), and anti CD235a/glycophorin A PE-conjugated (clone GA-R2-HIR2) were employed to evaluate the percentages of the main blood components (platelets, and erythrocytes) in the basic and static test of hemocompatibility, to obtain flow cytometric quantitative data. The samples were acquired by a FACSCanto II (BD) flow cytometer and the data was analyzed by Kaluza software (Beckman Coulter).

2.5.10. Flow cytometric DNA content evaluation on ethanol-fixed cells

Samples were fixed with cold 70 % ethanol (−20 °C) and stored at 4 °C until the analyses, the samples were washed at least twice with PBS [28]. The cell pellet was then resuspended in PBS containing propidium iodide (PI) 1 mg/mL and RNase 1 mg/mL. Finally, the sample was placed in a thermostatic bath at 37 °C for at least 30 min until the acquisition.

2.5.11. Confocal microscopy

Cells labeled with the same aforementioned probes for Flow Cytometric analyses were also analyzed by confocal microscopy. Analyses were performed with a Leica TCS SP5 II confocal microscope (Leica Microsystem, Germany) with 488, 543, and 633 nm lasers. The images obtained were analyzed by the Leica Application Suite Advanced Fluorescence (LASAF) and ImageJ software (NIH, UK). Indeed, to monitor cell morphology and contact points between keratin fibers and HT29, cells were analyzed, without any manipulation and detachments, using phase contrast microscopy [29]. The bright-field microscopy images were acquired by an optical inverted microscope using the 10× objective with data acquisition software (Nikon ECLIPSE TS100, software NIS-Elements F, Nikon Europe BV, Amstelveen, The Netherlands).

2.5.12. Blood smears

Blood smear evaluation can characterize the morphology of all cell lines. We employed K3 EDTA anticoagulated fresh blood for our tests. Briefly, using lens paper, we removed any dust from the main glass slide, placing the edge of the other slide at an approximately 35–45^0 angle in front of the blood drop. The second slide was gently pulled back into the blood drop, allowing the blood to spread to the edge of the slide. Care was taken to keep gentle, equal pressure throughout the whole process. After preparation, the smears were labeled by HEMOFAST (a modified Wright Solution, classically a mixture of eosin red and methylene blue dyes) and air-dried [30,31]. Observations were conducted by optical inverted microscope using the 40× objective with data acquisition software (Nikon ECLIPSE TS100, software NIS-Elements F, Nikon Europe BV, Amstelveen, The Netherlands). On the images (6 pictures for each of the three donor samples) erythrocyte aggregation and shape alteration were counted and reported as statistics.

3. Results and discussion

3.1. Correlations between the process parameters and morphology of the samples

In Fig. 2 the morphologies of the samples obtained by implementing the runs listed in Table 1 are shown. As observed, fibrous structures are produced only with the solutions containing the PEO 900 kDa. The effects of the process parameters as well as of their interactions on the samples' morphology are summarized Table 2. The mathematical model correlating the input factors with the output result (sample morphology) was refined through the *p-values* associated with the mathematical model as well as to the factors composing it, the regression coefficients R^2, adjusted-R^2 (adj-R^2), and predicted R^2 (pred-R^2). The adj-R^2 is the R^2 adjusted for the number of model terms, and it decreases as irrelevant terms are added. The pred-R^2value indicates how well future observations may be predicted. Adj-R^2 and pred-R^2 should be in reasonable agreement with each.

other: the rule of thumb is that the mathematical model is validated if they do not differ by >0.2 [32]. As can be seen, the complete model which considers the main factors and two interaction factors, is characterized by a *p-value* <0.005, implying that the model is significant. However, among the factors, only the X_1, X_2, X_4, and X_1X_2 are significant (*p*-value <0.05). Moreover, the Pred-R^2 is not as close to the Adj-R^2 (the difference is >0.2), therefore the model was reduced by eliminating the non-significant factors. Compared to the complete model, the reduced model shows an improved reliability of the fitting by showing a alower *p-value* (< 0.0001). The Adj-R^2 and Pred-R^2 of the reduced model are in reasonable agreement (their difference is <0.2), thereby meaning that the model can be used to predict responses for new observations.

The response surface graphs related to the refined mathematical model (Eq. 2) are shown in Fig. 3. As observed, the PEO molecular weight and the air pressure are the main factors affecting the SBS process of keratin-based formulations. In particular, the spinnability of keratin-based solutions improves with increasing the PEO molecular weight; on the contrary, it appears to worsen with increasing air pressure. A slight improvement can be observed with increasing the needle-collector distance, while a variation of the solution feed rate between 0.05 and 0.2 does not affect the spinnability process.

Based on the obtained results, the process conditions selected for the further development of the keratin fibrous patches were the PEO 900 kDa (2%*w/V*), an air pressure of 2 bar, a needle-collector distance of 30

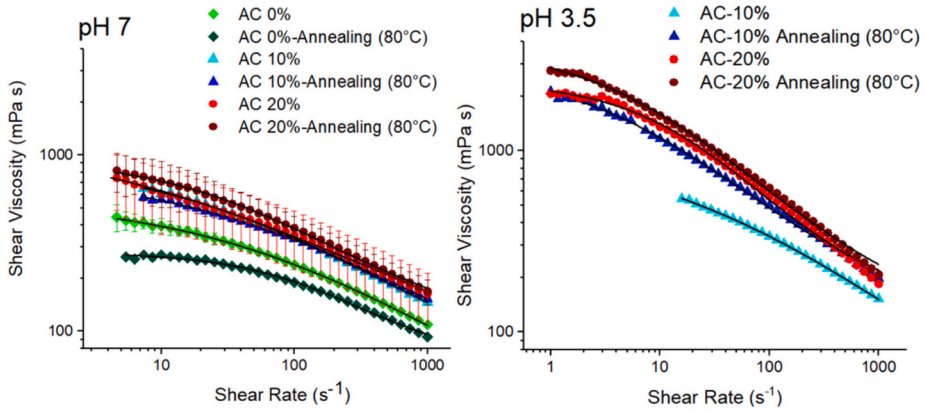

Fig. 4. Shear viscosity of the keratin based solutions at different contents of citric acid (AC) and different pH.

Table 3
Cross model parameters.

Sample	$\eta_0 (mPa\,s)$	n	$\lambda\,(s)$	R^2
AC 0 %	557 ± 18	0.52 ± 0.04	0.019 ± 0.001	0.999
AC 0 %-annealing (80 °C)	281 ± 3	0.93 ± 0.07	0.069 ± 0.005	0.996
AC 10 %-pH 7	929 ± 45	0.56 ± 0.04	0.033 ± 0.004	0.999
AC 10 %-pH 7-annealing (80 °C)	802 ± 41	0.50 ± 0.04	0.022 ± 0.002	0.999
AC 20 %-pH 7	1247 ± 96	0.50 ± 0.05	0.11 ± 0.003	0.996
AC 20 %-pH 7-annealing (80 °C)	975 ± 19	0.68 ± 0.03	0.029 ± 0.001	0.998
AC 10 %-pH 3.5	1024 ± 87	0.46 ± 0.04	0.46 ± 0.04	0.999
AC 10 %-pH 3.5-annealing (80 °C)	2827 ± 236	0.62 ± 0.04	0.203 ± 0.03	0.997
AC 20 %-pH 3.5	2391 ± 57	0.78 ± 0.04	0.073 ± 0.004	0.997
AC 20 %-pH 3.5-annealing (80 °C)	3753 ± 136	0.65 ± 0.03	0.18 ± 0.02	0.998

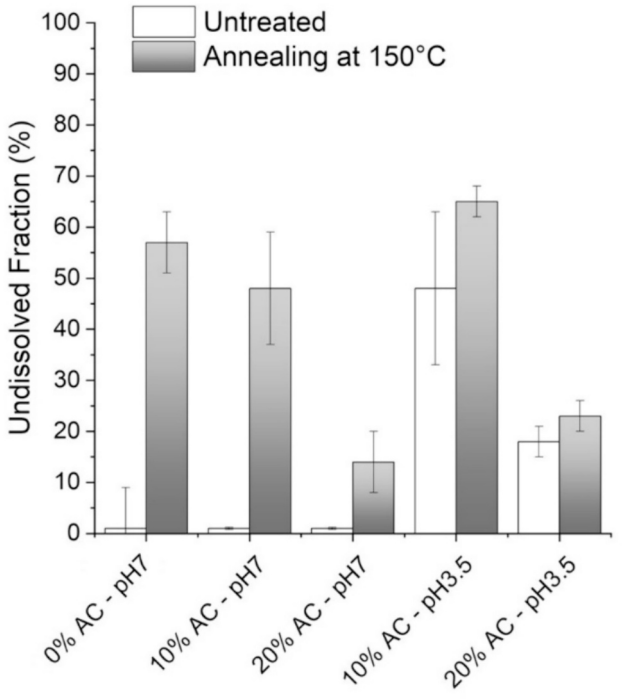

Fig. 5. Solubility percentages of the samples without citric acid (AC) and crosslinked with different amounts of citric acid (AC), untreated and annealed at 150 °C. The assay was performed in triplicate. Error bars represent the standard deviation.

cm, and solution feed rate of 0.125 mL/min (halfway in the considered values range). The visual appearance of the patches obtained with the aforementioned process conditions is shown in Fig. 2 **b**, while the SEM image is in Fig. 2c.

$$Y = 0.004792X_1 - 0.1979X_2 + 0.0417X_4 - 0.00052X_1X_2 + 0.8333 \quad (2)$$

3.2. *Effect of crosslinking on viscosity*

The influence of the citric acid, of the annealing process at 80 °C, as well as of the pH on crosslinking was monitored by measuring the apparent viscosity (shear viscosity) as a function of the shear rate (Fig. 4). As shown in Fig. 4, all the samples show non-Newtonian shear-thinning (pseudoplastic) behavior. The Cross model was used to fit the shear viscosity-shear rate data (Eq. 3):

$$\frac{\eta - \eta_\infty}{\eta_0 - \eta_\infty} = \frac{1}{1 + (\lambda\dot{\gamma})^n} \quad (3)$$

where, $\eta_0\ (mPa\,s)$ is the zero-shear viscosity (the apparent viscosity at any shear rate) and $\eta_\infty\ (mPa\,s)$ is the viscosity at very high shear rate, $\lambda\ (s)$ is the characteristic relaxation time (that approximately corresponds to the reciprocal related to the shear thinning onset), while n characterizes the slope of the line over the shear-thinning region [33].

The right balance between the zero-shear viscosity, the shear thinning, and the relaxation time is crucial for the blow spinning process. A relatively high η_0 is desirable to have a stable drop of the polymer solution at the needle; while a relatively high value for n indicates a significant shear thinning behavior which favors the alignment of the polymer chains and therefore the jet thinning when subjected to the shear stress induced by the gas flow. Finally, a relatively high λ indicates a slower relaxation dynamic of the polymer chains, meaning that they better maintain the stretching imparted by the gas flow.

The obtained Cross model parameters are summarized in Table 3. The high R^2 indicates that the shear viscosity data are well fitted by the Cross model. All n values were ≥ 0.5, indicating that the polymer solutions exhibit non-Newtonian shear-thinning behavior. As shown, the η_0 increases with increasing the citric acid content and with decreasing the pH. The annealing at 80 °C increases the η_0 at acidic pH; while an opposite trend is observed at a neutral pH. This suggests that the crosslinking mediated by citric acid is more efficient at acidic pH and it is enhanced by the annealing process. This behavior was also observed by several authors and it has been attributed to the formation of reactive cyclic anhydride [34]. Moreover, the solutions containing the 10 % of citric acid at pH 3.5, both untreated and annealed, show higher λ values suggesting a slower relaxation dynamic of the polymer chains, probably due to the enhanced crosslinking degree occurring at these conditions.

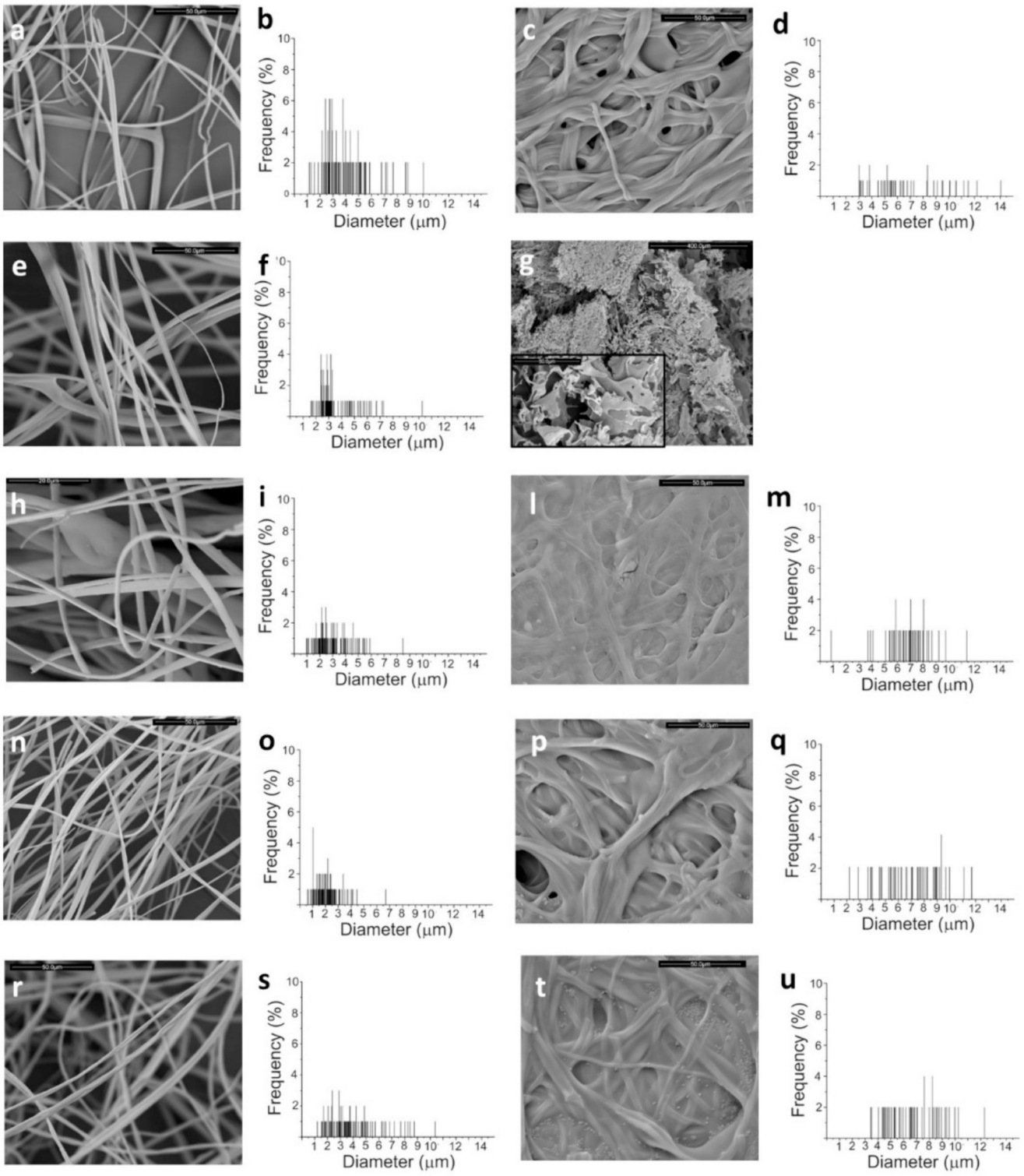

Fig. 6. SEM images of: 0 % citric acid (a); 0 % citric acid immersed in water (c); 10 % citric acid, pH 7 (e); 10 % citric acid, pH 7, immersed in water (g); 20 % citric acid, pH 7 (h); 20 % citric acid, pH 7, immersed in water (l); 10 % citric acid, pH 3.5 (n); 10 % citric acid, pH 3.5, immersed in water (p); 20 % citric acid, pH 3.5 (r); 20 % citric acid, pH 3.5, immersed in water (t); Diameter distribution of 0 % citric acid (b); 0 % citric acid immersed in water (d); 10 % citric acid, pH 7 (f); 10 % citric acid, pH 7, immersed in water (i); 20 % citric acid, pH 7 (m); 20 % citric acid, pH 7, immersed in water (o); 10 % citric acid, pH 3.5 (q); 10 % citric acid, pH 3.5, immersed in water (s); 20 % citric acid, pH 3.5 (r); 20 % citric acid, pH 3.5, immersed in water (u).

3.3. Effect of crosslinking on water stability of the spun patches

The effects of acid-citric mediated crosslinking at different pH and of the post-annealing at high temperature (150 °C for 5 min) on the water stability of the samples are summarized in Fig. 5. The keratin/PEO fibrous patch containing no citric acid was considered as the reference sample.

As can be seen in Fig. 5, the annealing at 150 °C for 5 min contributes to improving the water stability of non-woven patches. Indeed, the fraction of the annealed reference sample (0 % AC, pH 7) that remains

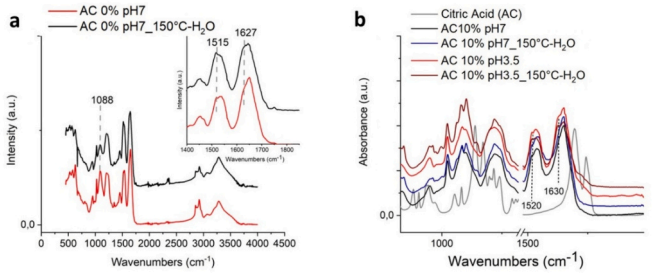

Fig. 7. FTIR spectra of the keratin non-woven mats a) without citric acid, untreated and annealed at 150 °C and immersed in water; b) with 10 % of citric acid at different pH, untreated and annealed at 150 °C and immersed in water.

undissolved in water is 57 ± 6 %; while the corresponding unannealed one almost totally dissolves in water. This behavior, also observed by Varesano et al., has been attributed to the protein crosslinking through the reaction of the amino and carboxyl groups of the protein side chains, which occurs at high temperatures [35].

As regards the effect of crosslinking with AC on the water stability of the samples, non-woven patches treated with different amounts of AC at pH 7 and not annealed at 150 °C, completely dissolve in water, indicating that the crosslinking did not occur. Instead, samples treated with different amounts of AC at pH 3.5 and not annealed at 150 °C, show increased water stability, suggesting the occurrence of crosslinking with AC. The undissolved fraction is 48 ± 15 % for the unannealed sample crosslinked with the 10 % wt of AC, and 18 ± 3 % for the one crosslinked with the 20%wt of AC.

As expected, the annealing of the samples containing different amounts of AC at both pH 7 and pH 3.5 increases their water stability. Nevertheless, under the same process conditions (untreated and annealed at 150 °C), the sample containing 10 % wt of AC shows the greatest water stability. This behavior supports the hypothesis of a greater degree of crosslinking at these conditions of AC content and pH, in agreement with the results of rheological tests.

3.4. Effect of crosslinking on the morphology of the fibers

In Fig. 6, SEM images and diameter distribution graphs of all the samples are reported. The untreated fibers are defect-free and their diameters range from 1 to 10 μm. Notwithstanding its higher zero-shear viscosity, the solution containing the 10 % citric acid at pH 3.5 produces the thinnest fibers (Fig. 6 **n and o**). This could be attributed to the highest relaxation time of the polymer chains (highest λ value), which allows them to maintain the stretching imparted during the spinning process.

As expected, when immersed in water, the fibers tend to swell and stick together. However, except for the sample containing 10 % citric acid at pH 7 (Fig. 6 **g**), all the other samples maintain the fibrous structure, even if the relative distribution of diameters shifts and widens towards higher diameter values (until it reaches 15 μm in diameter).

3.5. Crosslinking mechanism

The cross-linking of keratin in the prepared samples can occur through two possible mechanisms. The first mechanism (thermal cross-linking) does not involve citric acid and consists of the amide bond formation between carboxylic acids and amino groups of the protein side chains, which occurs at a temperature higher than 120 °C [35,36]. The second mechanism (cross-linking with AC) requires citric acid and consists of a nucleophilic acyl substitution between citric acid and keratin and/or PEO [37]. This reaction results in the formation of covalent bonds between carboxylic groups of the citric acid and N—H or O—H groups of the keratin and PEO [38]. On the base of the rheological and water stability behavior of the samples, this crosslinking mechanism seems to be more effective upon annealing at 80 °C and under acidic pH.

Fig. 7a shows the spectra of the Keratin/PEO fibrous patches before and after the heating treatments at 150 °C, followed by immersion in water. The spectrum of the untreated keratin patches shows the characteristic adsorption bands of the keratin, such as: amide A band (3300 cm^{-1}) assigned to the N—H stretching vibrations, amide I band (1650 cm^{-1}) associated with the C═O stretching vibrations, amide II band (1540 cm-1) related to the in-plane bending modes of N—H bonds with some contributions of C—N stretching vibrations, and amide III band (1200 cm^{-1}), a complex band associated to an in-phase combination of N—H in-plane bending, C—N stretching vibrations, and C═O bending vibrations. In addition, the peak at 1025 cm^{-1} is attributed to the cysteine-S-sulfonated residues formed during the extraction process of keratin by sulphitolysis [36] [35]. Instead, the peak at 1088 cm^{-1} is correlated to the C-O-C stretching vibration of the PEO [39].

As observed in the box of Fig. 7a, the sample heated at 150 °C shows a more intense shoulder at 1620 cm^{-1} and 1515 cm^{-1} of the Amide *I* and

Table 4
Adhesive properties of keratin spun patches.

Sample	Adhesive force (N)	Elongation at detachment (mm)	Work of adhesion (AUC) (N•mm^2)
Untreated	0.86 ± 0.01	49.97 ± 0.02	2.69 ± 0.02
Thermally stabilized at 150 °C	1.15 ± 0.03	12.20 ± 0.03	0.36 ± 0.07

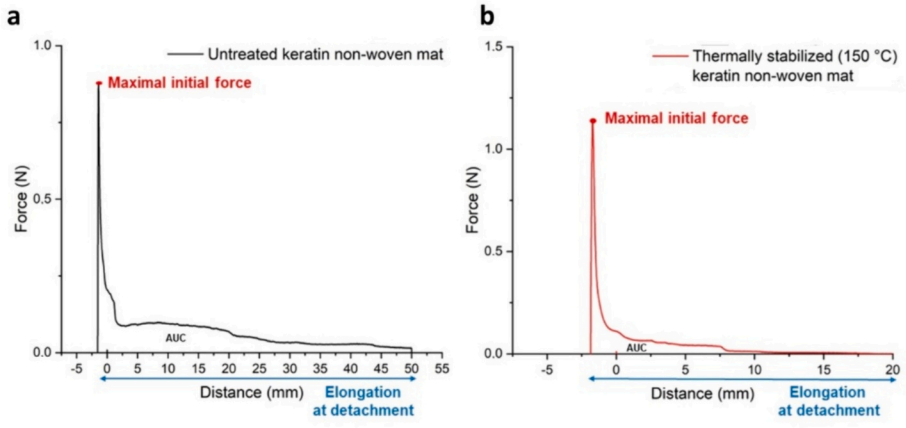

Fig. 8. Adhesion graph of keratin spun patches and evaluated parameters of the force-distance curve. The AUC is the area under the curve.

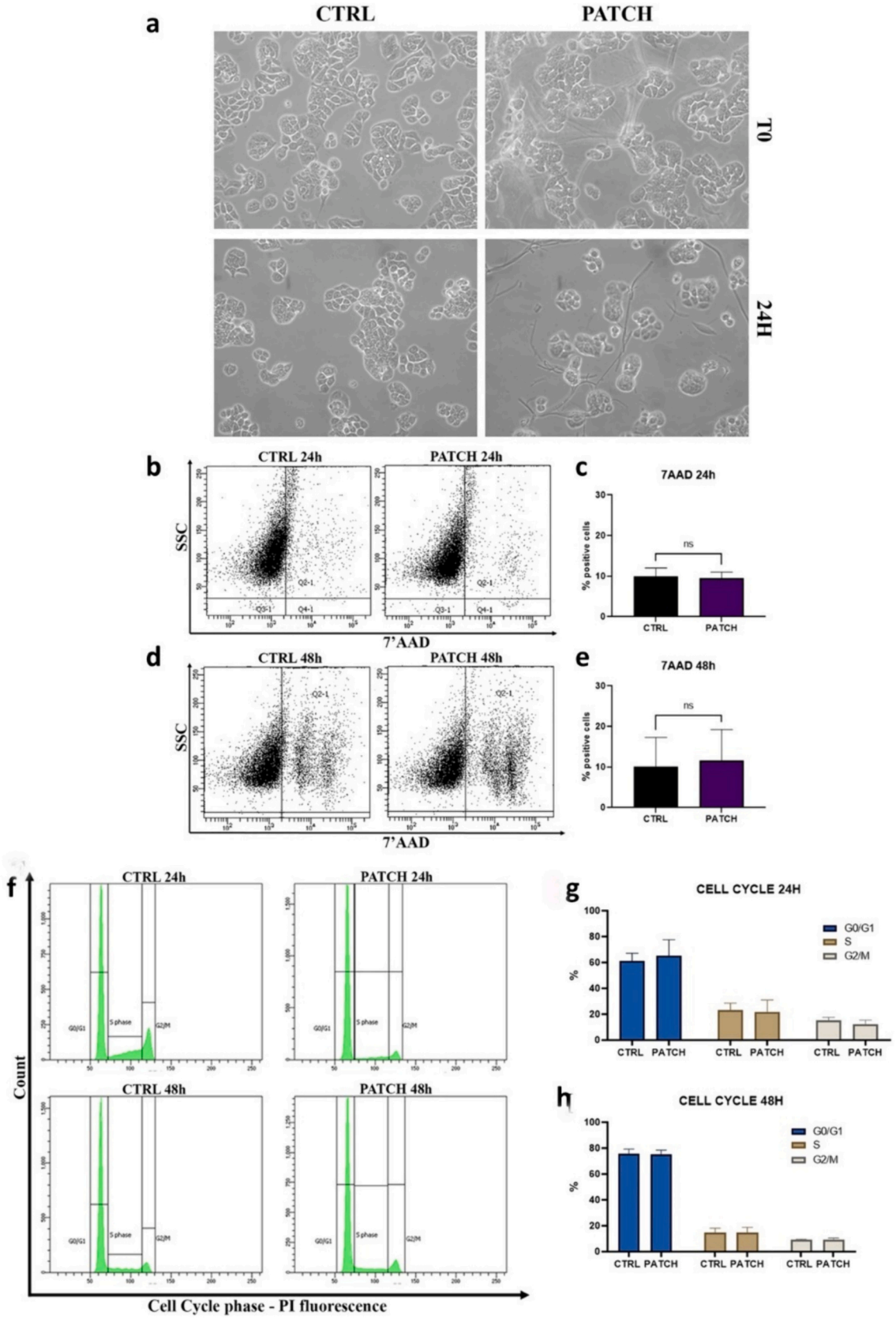

Fig. 9. (a): Light inverted microscope images from HT-29 control cells and HT-29 treated with the patch, highlight that part of the keratin filaments are close to cell clusters and that cells also adhere in their proximity or on their structure. (b): Dot plot 7-AAD vs SSC from control and patch-treated samples, after 24 h (b) and 48 h (d). Percentages of 7'AAD positive cells of control and patch-treated samples, after 24 h (c) and 48 h (e). (f) Cytometric histograms for the cell cycle distribution for control and patch treated cells at 24 h and 48 h), with relative percentages histogram of cells in cell cycle phases at 24 h (g) and 48 h (h).

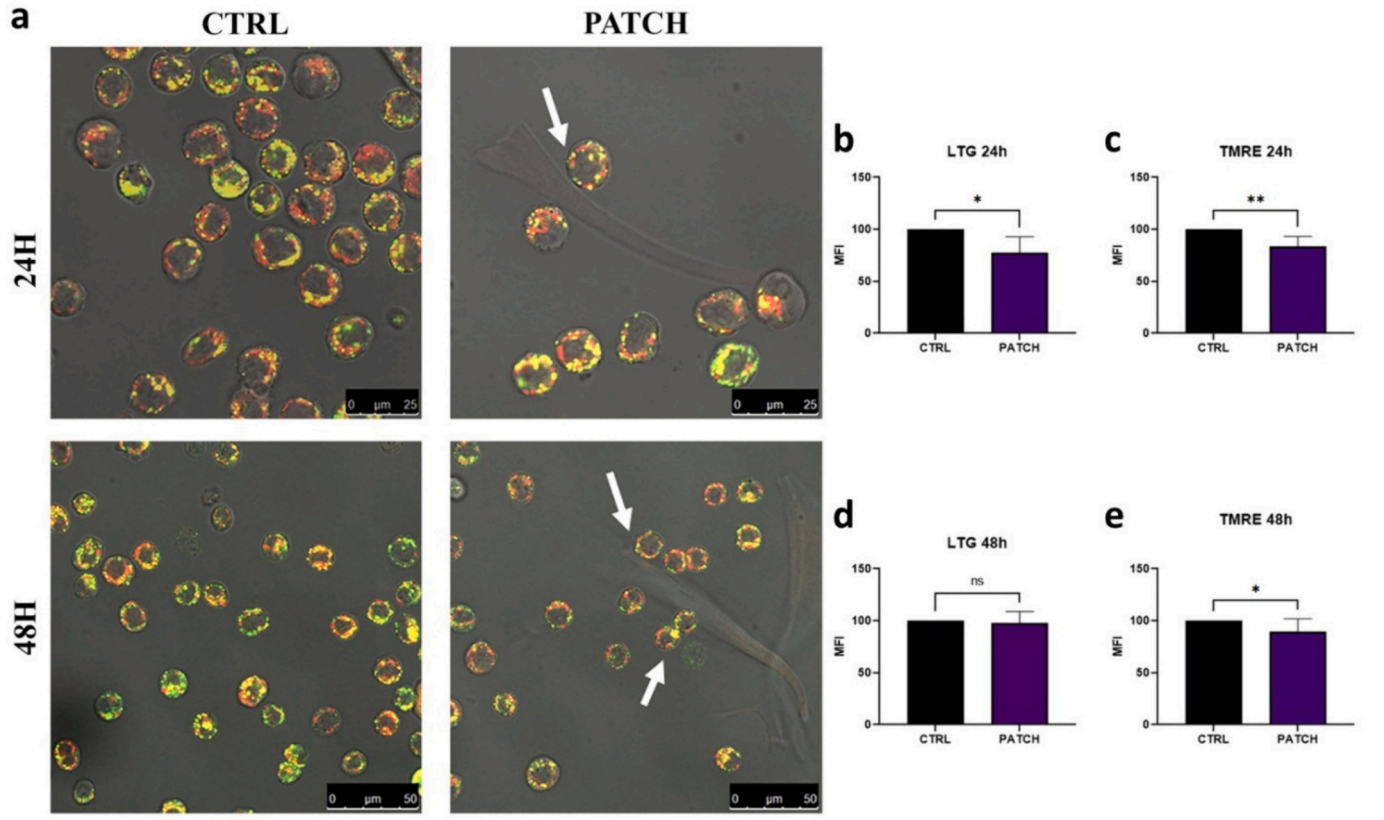

Fig. 10. a) Merged image of green (LysoTracker Green), red (TMRE), and bright field channels for ctrl and patch treated cells, observed at the confocal microscope. White arrows show cells adherent to keratin fiber. Histograms of MFI variations of LTG and TMRE calculated after 24 h(b,c) and 48 h (d,e). (For interpretation of the references to colour in this figure legend, the reader is referred to the web version of this article.)

II, respectively. This may be due to an increased packing of the protein chains resulting from the crosslinking that occurs through the formation of amide bonds between the free amino groups of lysine and the free carboxyl groups of glutamic and aspartic acids (thermal crosslinking) [35]. This higher packing reduces the vibrations energy of some C═O groups of the proteins causing a shift at lower wavenumbers of the relative adsorption band. Moreover, compared to the untreated sample, the intensity of the peak at 1088 cm^{-1} of the thermally crosslinked sample immersed in water is significantly reduced (Fig. 7a). This suggests that during the soaking in water, part of the PEO is released from the sample.

In the presence of citric acid (Fig. 7 b), it can be observed that the sample obtained from the solution at pH 3.5 has the shoulders at 1630 cm^{-1} and 1515 cm^{-1} of the amides I and II, respectively. Also in this case, the presence of the shoulders at 1630 cm^{-1} and 1515 cm^{-1} could be ascribed to a higher packing of the polymer chains induced by the crosslinking with citric acid and/or an α-β transition of keratin, usually observed in acidic environments [36]. Nevertheless, these shoulders are not present in the samples obtained from solutions at pH 7, both untreated and thermally treated at 150 °C and immersed in water, indicating that the cross-linking with AC does not occur at a neutral.

3.6. Adhesion of the spun patches

Adhesive properties of keratin spun patches were evaluated through a probe tack test using a texture analyzer. This test allows the measurement of the adhesive force, elongation at detachment, and work of adhesion of the investigated material from the resulting force-distance curves (Fig. 8). Briefly, the adhesive force represents the maximal initial force for detachment (peak force) while the work of adhesion (area under the curve, AUC) indicates the total work required throughout the withdrawal of the stainless-steel probe [40]. As can be seen in Table 4, thermal stabilization at 150 °C of the sample leds to a reinforcement of the matrix, increasing the maximal initial force for detachment. Nevertheless, the untreated sample shows a higher elongation at the break and a greater AUC than the thermally stabilized one. In this case, AUC is mainly influenced by the facilitated fibrillation of the untreated keratin spun patch and follows the same trend of elongation at the break parameter [41]. Overall, given the potential biomedical application of these samples, the adhesive strength under 3.7 N allows for their painless removal from the tissues [38]. Finally, the steeper slope on the right side of the curve of both samples (Fig. 8) suggests they have sufficient rigidity to not deform due to stress received during application [42].

3.7. Cytotoxicity studies

The first analyses in this pilot study were conducted using an inverted microscope, to verify if keratin filamentous structures were visible and able to settle on the bottom, interacting with the adherent cell layer, since a part of the patch fragments is observable floating in the medium (Fig. 9a). Flow cytometry allows the detection of a negligible cytotoxic effect after 24 h and 48 h. However, it is possible to observe that spontaneous apoptotic/necrotic cells, detected after 48 h in the control sample, slightly alter their distribution suggesting increased membrane damage in those cells normally 7AAD positive (yet damaged) in control cultured cell lines (Fig. 9 b-e).

Furthermore, to take into consideration not only possible cell death induction but also inhibition of proliferation, we evaluated DNA content profiles after 24 h and 48 h (Fig. 9 f): with this preliminary approach we can evaluate eventual subdiploid peak and, particularly, cell cycle phases. After 24 h we observed a decrease in percentages of S and G2/M

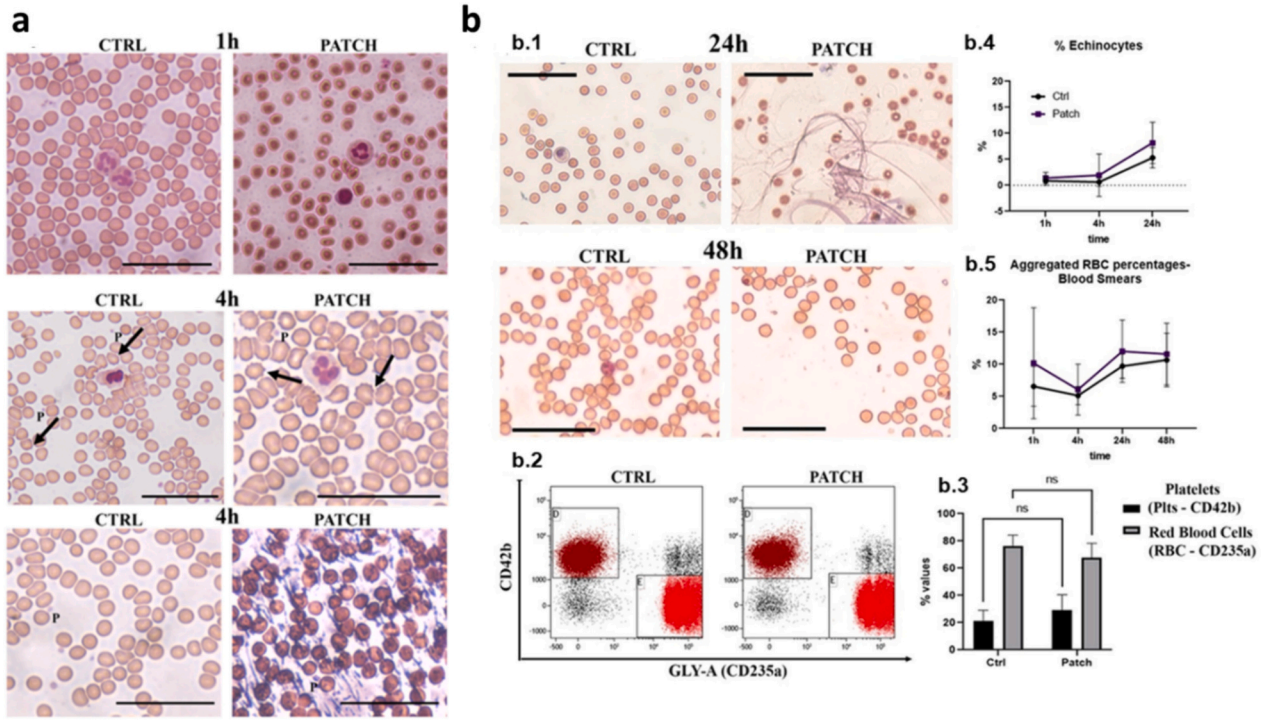

Fig. 11. Evidence of erythrocyte and erythrocyte aggregates observed by conventional optical microscopy in control samples and under the influence of the washed keratin patches. Since only 4–5 μl of blood are used to prepare the smear, keratin filaments are appreciable only in some preparations. **a)** White blood cells, similar in both control and patch-treated samples, are visible. Echinocytes are indicated by black arrows while platelets are indicated by P. **b)** Keratin filaments are appreciable in a selected smear after 24 h. Platelets and erythrocytes are traced also by mAb labeling, highlighting similar profiles and no antigenicity disturbance by the foreign keratin materials. Statistics histogram reports percentages of Echinocytes and RBC aggregates by two-way Anova tests. *V*alues were obtained by counting cells from 6 images from three different donors, for both control and patch treated cells.

phases, indicating a mild inhibition of cell proliferation, compared to control cells (Fig. 9 g). Of note, after 48 h, cell cycle phases result similarly in both control and patch-treated cells, suggesting a complete restoration of proliferative ability (Fig. 9 h). Lysosomal and mitochondrial networks were studied by LTG and TMRE labeling in cytometric and confocal settings (Fig. 10). At 24 h, both lysosomal and mitochondrial organelles seem to be involved after patch treatments (Fig. 10 **a-c**): this impact is revealed by the decrease in MFI (Mean Fluorescence Intensity) observed by quantitative flow cytometric data and confirmed by confocal images. As detected for cell cycle evaluation, lysosomal and mitochondrial functions appear almost completely restored after 48 h.

3.8. Basic hemocompatibility results

Erythrocyte aggregation is mainly due to the discord morphology and electrostatic interactions between erythrocytes Smears made immediately after the addition of anticoagulant did not show any artefactual changes. However, during our tests from T0 to 48 h, control, and patch-treated samples were monitored step by step (Fig. 11a and b.**1**), reporting aggregates and morphologic differences during time (Fig. 11b.**2**), mainly caused by aging. Indeed, it is possible to observe some echinocytes also in storage-aged control samples (24 h) with slight, no significant increase, in patch-treated samples (n = 3 donors) (Fig. 11b.**3**). RBCs' shape and membrane rigidity play critical roles in their quality, function, and fate, such as gas transport capacity and RBC clearance from circulation [37]. The morphology of RBCs progressively deteriorates throughout storage time [38]. This is the reason we also investigated the presence of RBC and platelets specific markers by Flow Cytometry at 48 h (Fig. 11b.**4**), finding no apparent antigenicity disturbance on recognizing CD42b and CD235 surface antigens, induced by keratin patches, and no significant differences in control and patch-treated samples (Figs. 11b.**5**). Another cellular constituent of blood is represented by leukocytes. These cells (subdivided into monocytes, granulocytes, and lymphocytes) play a critical role in inflammation, immunity, and host defense systems and are often overlooked in terms of contribution to hemostasis. Fig. 11a and b highlight leukocytes from both control and patch-treated samples, with similar morphology, after 1 h, 4 h, 24, and 48 h.

4. Conclusion

The present work developed a strategy to re-ennoble wool keratin wastes into advanced materials for biomedical applications. Indeed, the solution blow spinning process of keratin extracted from wool wastes into patches made of randomly oriented microfilament has been set up for the first time. Aqueous solutions of the HMW keratin have been formulated to realize a process suitable also for the in-situ deposition of the keratin patches. The 2-level full factorial design used for the screening of the most influencing process parameters revealed that the formation of filaments occurs when polyethylene oxide (900 kDa) at 2 % *w/V* is added to the keratin aqueous solution. Moreover, a pressure of 2 bar is needed for the stretching of keratin chains into filament as well as a needle-target distance of 30 cm to ensure the complete aqueous evaporation before the fibers reach the collector. Instead, a solution feed rate ranging from 0.05 to 0.2 mL/min seems to not influence the process.

The morphology and the water stability of the keratin spun patches are highly dependent on the amount of citric acid added to the keratin solutions as well as on the annealing processes performed on the solutions before spinning and on the spun samples. An amount of 10 % of citric acid versus keratin is sufficient to crosslink the keratin chains and the degree of crosslinking seems to increase at acidic pH 3.5 and after annealing the solutions at 80 °C for 15 min. In fact, in these conditions there is a significant increase in the shear viscosity of the solutions, and, at the same time, an increased undissolved fraction is observed when the

patch is immersed in water for 24 h. The post annealing of the keratin filaments at 150 °C for 5 min contributes to increasing the water stability of the patches. According to the FTIR analysis, crosslinking with citric acid occurs through the formation of amide bonds between the keratin and the acid, which increases the packing of the protein chains. As regards the adhesion properties of the patches, although heat treatment at 150 °C helps to increase the initial force for detachment from the application surface, it reduces the elongation at break and the total work required for the withdrawal of the patches from the surface. This means that even the patches that cannot be thermally treated, such as those deposited in situ, display excellent adhesion properties. The spun keratin patches did not show any significant toxic effects on either HT29 epithelial cells or human blood cells.

Therefore, the solution-blowing process developed for HMW keratin could be a valuable process for the production of patches, which can also be deposited in situ and need to be blood-contacting, representing a starting point for specific biomedical applications, e.g. for the treatment of intestinal epithelium injuries.

Supplementary data to this article can be found online at https://doi.org/10.1016/j.ijbiomac.2024.133722.

CRediT authorship contribution statement

Giorgia Maurizii: Writing – original draft, Validation, Methodology, Investigation, Formal analysis, Data curation. **Laura Valentini:** Investigation. **Giovanna Sotgiu:** Writing – review & editing, Resources, Investigation. **Roberto Zamboni:** Writing – review & editing, Resources. **Cinzia Tonetti:** Writing – review & editing, Investigation. **Claudia Vineis:** Writing – review & editing, Investigation. **Barbara Canonico:** Writing – original draft, Validation, Methodology, Investigation, Formal analysis, Data curation. **Mariele Montanari:** Writing – original draft, Validation, Investigation, Formal analysis. **Mattia Tiboni:** Writing – review & editing, Methodology, Investigation. **Luca Casettari:** Writing – review & editing, Validation, Resources, Funding acquisition. **Annalisa Aluigi:** Writing – original draft, Validation, Supervision, Project administration, Methodology, Data curation, Conceptualization.

Declaration of competing interest

On behalf of all authors, the corresponding author states that there is no conflict of interest.

Data availability

The raw/processed data required to reproduce these findings cannot be shared at this time as the data also forms part of an ongoing study.

Acknowledgment

This work has been carried out within an institutional research of the Department of Biological Macromolecules - University of Urbino (DISB_ALUIGI_PROGETTO_AZIONE_PSD_2021_2023).

The authors also acknoledge the European Union - Next Generation EU - PNRR MUR project ECS_00000041-VITALITY"; and the ITIS E. Mattei (Urbino, PU, Italy) for the utilization of the FTIR instrument.

References

[1] B.-D. Chereji, F.-D. Munteanu, The impact of sheep waste wool on the environment, SCIENTIFIC PAPERS-SERIES E-LAND RECLAMATION EARTH OBSERVATION & SURVEYING ENVIRONMENTAL ENGINEERING 11 (2022) 458–463.

[2] B. Petek, R. Marinšek Logar, Management of waste sheep wool as valuable organic substrate in European Union countries, J Mater Cycles Waste Manag 23 (2021) 44–54, https://doi.org/10.1007/s10163-020-01121-3.

[3] I. Chukwunonso Ossai, F. Shahul Hamid, A. Hassan, Valorisation of keratinous wastes: a sustainable approach towards a circular economy, Waste Manag. 151 (2022) 81–104, https://doi.org/10.1016/j.wasman.2022.07.021.

[4] L.M. Dowling, W.G. Crewther, A.S. Inglis, The primary structure of component 8c-1, a subunit protein of intermediate filaments in wool keratin, Relationships with proteins from other intermediate filaments, Biochemical Journal 236 (1986) 695–703, https://doi.org/10.1042/bj2360695.

[5] J. Zhu, N. Ma, S. Li, L. Zhang, X. Tong, Y. Shao, C. Shen, Y. Wen, M. Jian, Y. Shao, J. Zhang, Reinforced wool keratin fibers via dithiol chain re-bonding, Adv. Funct. Mater. 33 (2023), https://doi.org/10.1002/adfm.202213644.

[6] T. Posati, A. Listwan, G. Sotgiu, A. Torreggiani, R. Zamboni, A. Aluigi, Keratin/Hydrotalcites hybrid sponges as promising adsorbents for cationic and anionic dyes, Front. Bioeng. Biotechnol. 8 (2020), https://doi.org/10.3389/fbioe.2020.00068.

[7] S. Khorshid, R. Goffi, G. Maurizii, S. Benedetti, G. Sotgiu, R. Zamboni, S. Buoso, R. Galuppi, T. Bordoni, M. Tiboni, A. Aluigi, L. Casettari, Microfluidic manufacturing of tioconazole loaded keratin nanocarriers: development and optimization by design of experiments, Int. J. Pharm. 647 (2023) 123489, https://doi.org/10.1016/j.ijpharm.2023.123489.

[8] X. Hu, P. Cebe, A.S. Weiss, F. Omenetto, D.L. Kaplan, Protein-based composite materials, Mater. Today 15 (2012) 208–215, https://doi.org/10.1016/S1369-7021(12)70091-3.

[9] E. Ranjit, S. Hamlet, R. George, A. Sharma, R.M. Love, Biofunctional approaches of wool-based keratin for tissue engineering, Journal of Science: Advanced Materials and Devices 7 (2022) 100398, https://doi.org/10.1016/j.jsamd.2021.10.001.

[10] J. Zhu, N. Ma, S. Li, L. Zhang, X. Tong, Y. Shao, C. Shen, Y. Wen, M. Jian, Y. Shao, J. Zhang, Reinforced wool keratin fibers via dithiol chain re-bonding, Adv. Funct. Mater. 33 (2023), https://doi.org/10.1002/adfm.202213644.

[11] G. Cao, M.Z. Rong, M.Q. Zhang, Continuous high-content keratin fibers with balanced properties derived from wool waste, ACS Sustain. Chem. Eng. 8 (2020) 18148–18156, https://doi.org/10.1021/acssuschemeng.0c06530.

[12] J.-P. Ye, J.-S. Gong, C. Su, Y.-G. Liu, M. Jiang, H. Pan, R.-Y. Li, Y. Geng, Z.-H. Xu, J.-S. Shi, Fabrication and characterization of high molecular keratin based nanofibrous membranes for wound healing, Colloids Surf. B: Biointerfaces 194 (2020) 111158, https://doi.org/10.1016/j.colsurfb.2020.111158.

[13] Y. Liu, Q. Guo, X. Zhang, Y. Wang, X. Mo, T. Wu, Progress in electrospun fibers for manipulating cell behaviors, Adv. Fiber Mater. 5 (2023) 1241–1272, https://doi.org/10.1007/s42765-023-00281-9.

[14] J. Liu, T. Cui, X. Xu, Y. Du, L. Wang, S. Chen, J. Pang, Robust alcohol soluble polyurethane/chitosan/silk Sericin (APU/CS/SS) nanofiber scaffolds toward artificial skin extracellular matrices via microfluidic blow-spinning, Adv. Fiber Mater. 5 (2023) 349–361, https://doi.org/10.1007/s42765-022-00227-7.

[15] X. Yan, M. Yu, S. Ramakrishna, S.J. Russell, Y.-Z. Long, Advances in portable electrospinning devices for *in situ* delivery of personalized wound care, Nanoscale 11 (2019) 19166–19178, https://doi.org/10.1039/C9NR02802A.

[16] Y. Gao, H.-F. Xiang, X.-X. Wang, K. Yan, Q. Liu, X. Li, R.-Q. Liu, M. Yu, Y.-Z. Long, A portable solution blow spinning device for minimally invasive surgery hemostasis, Chem. Eng. J. 387 (2020) 124052, https://doi.org/10.1016/j.cej.2020.124052.

[17] R. Leardi, Experimental design in chemistry: a tutorial, Anal. Chim. Acta 652 (2009) 161–172, https://doi.org/10.1016/j.aca.2009.06.015.

[18] K.D. Boger, A.E. Sheridan, A.L. Ziegler, A.T. Blikslager, Mechanisms and modeling of wound repair in the intestinal epithelium, Tissue Barriers 11 (2023), https://doi.org/10.1080/21688370.2022.2087454.

[19] E. Fröhlich, Comparison of conventional and advanced *in vitro* models in the toxicity testing of nanoparticles, Artif cells Nanomed, Biotechnol 46 (2018) 1091–1107, https://doi.org/10.1080/21691401.2018.1479709.

[20] D. Martínez-Maqueda, B. Miralles, I. Recio, HT29 Cell Line, in: The Impact of Food Bioactives on Health, Springer International Publishing, Cham, 2015, pp. 113–124, https://doi.org/10.1007/978-3-319-16104-4_11.

[21] J.E. Domínguez, E. Olivos, C. Vázquez, J.M. Rivera, R. Hernández-Cortes, J. González-Benito, Automated low-cost device to produce sub-micrometric polymer fibers based on blow spun method, HardwareX 10 (2021) e00218, https://doi.org/10.1016/j.ohx.2021.e00218.

[22] M. Weber, H. Steinle, S. Golombek, L. Hann, C. Schlensak, H.P. Wendel, M. Avci-Adali, Blood-Contacting Biomaterials: In Vitro Evaluation of the Hemocompatibility, Front Bioeng Biotechnol 6, 2018, https://doi.org/10.3389/fbioe.2018.00099.

[23] M. Weber, H. Steinle, S. Golombek, L. Hann, C. Schlensak, H.P. Wendel, M. Avci-Adali, Blood-Contacting Biomaterials: In Vitro Evaluation of the Hemocompatibility, Front Bioeng Biotechnol 6, 2018, https://doi.org/10.3389/fbioe.2018.00099.

[24] M. Nalezinková, In vitro hemocompatibility testing of medical devices, Thromb. Res. 195 (2020) 146–150, https://doi.org/10.1016/j.thromres.2020.07.027.

[25] M. Montanari, S. Burattini, C. Ciacci, P. Ambrogini, S. Carloni, W. Balduini, D. Lopez, G. Panza, S. Papa, B. Canonico, Automated—mechanical procedure compared to gentle enzymatic tissue dissociation in cell function studies, Biomolecules 12 (2022) 701, https://doi.org/10.3390/biom12050701.

[26] F. Sola, B. Canonico, M. Montanari, A. Volpe, C. Barattini, C. Pellegrino, E. Cesarini, M. Guescini, M. Battistelli, C. Ortolani, A. Ventola, S. Papa, Uptake and intracellular trafficking studies of multiple dye-doped Core-Shell silica nanoparticles in lymphoid and myeloid cells, Nanotechnol. Sci. Appl. 14 (2021) 29–48, https://doi.org/10.2147/NSA.S290867.

[27] B. Canonico, L. Giorgi, M.G. Nasoni, M. Montanari, G. Ambrosi, M. Formica, C. Ciacci, P. Ambrogini, S. Papa, V. Fusi, F. Luchetti, Synthesis and biological characterization of a new fluorescent probe for vesicular trafficking based on

polyazamacrocycle derivative, Biol. Chem. 402 (2021) 1225–1237, https://doi.org/10.1515/hsz-2021-0204.
[28] M. Montanari, M. Guescini, O. Gundogdu, F. Luchetti, P. Lanuti, C. Ciacci, S. Burattini, R. Campana, C. Ortolani, S. Papa, B. Canonico, Extracellular vesicles from campylobacter jejuni CDT-treated Caco-2 cells inhibit proliferation of tumour intestinal Caco-2 cells and myeloid U937 cells: detailing the global cell response for potential application in anti-tumour strategies, Int. J. Mol. Sci. 24 (2022) 487, https://doi.org/10.3390/ijms24010487.
[29] F. Sola, M. Montanari, M. Fiorani, C. Barattini, C. Ciacci, S. Burattini, D. Lopez, A. Ventola, L. Zamai, C. Ortolani, S. Papa, B. Canonico, Fluorescent silica nanoparticles targeting mitochondria: trafficking in myeloid cells and application as doxorubicin delivery system in breast Cancer cells, Int. J. Mol. Sci. 23 (2022) 3069, https://doi.org/10.3390/ijms23063069.
[30] D. de B. Welchman, H.L. Ainsworth, T.W. Pennycott, G. MacKenzie, A.M. Wood, Pheasant ataxia: a new condition in pheasant poults, Vet. Rec. 147 (2000) 93–97, https://doi.org/10.1136/vr.147.4.93.
[31] P. Di Francesco, R. Falchetti, R. Gaziano, G. Lanzilli, L. Belogi, G. Ravagnan, E. Garaci, Differential effects of short-term or prolonged cocaine exposure on peripheral blood cells in mice, Life Sci. 54 (1994) 2015–2020, https://doi.org/10.1016/0024-3205(94)90136-8.
[32] I.M. Fukuda, C.F.F. Pinto, C. dos S. Moreira, A.M. Saviano, F.R. Lourenço, Design of Experiments (DoE) applied to pharmaceutical and analytical quality by design (QbD), Brazilian, J. Pharm. Sci. 54 (2018), https://doi.org/10.1590/s2175-97902018000001006.
[33] K. Sungsanit, N. Kao, S.N. Bhattacharya, Properties of linear poly(lactic acid)/polyethylene glycol blends, Polym. Eng. Sci. 52 (2012) 108–116, https://doi.org/10.1002/pen.22052.
[34] M.H. Cumming, A.R. Leonard, D.S. LeCorre-Bordes, K. Hofman, Intra-fibrillar citric acid crosslinking of marine collagen electrospun nanofibres, Int. J. Biol. Macromol. 114 (2018) 874–881, https://doi.org/10.1016/j.ijbiomac.2018.03.180.
[35] A. Varesano, C. Vineis, C. Tonetti, D.O.S. Ramírez, G. Mazzuchetti, Chemical and physical modifications of electrospun keratin nanofibers induced by heating treatments, J. Appl. Polym. Sci. 131 (2014), https://doi.org/10.1002/app.40532.
[36] A. Aluigi, A. Corbellini, F. Rombaldoni, M. Zoccola, M. Canetti, Morphological and structural investigation of wool-derived keratin nanofibres crosslinked by thermal treatment, Int. J. Biol. Macromol. 57 (2013) 30–37, https://doi.org/10.1016/j.ijbiomac.2013.02.013.
[37] Q. Jiang, N. Reddy, S. Zhang, N. Roscioli, Y. Yang, Water-stable electrospun collagen fibers from a non-toxic solvent and crosslinking system, J. Biomed. Mater. Res. A 101A (2013) 1237–1247, https://doi.org/10.1002/jbm.a.34422.
[38] K. Arunprasert, C. Pornpitchanarong, T. Rojanarata, T. Ngawhirunpat, P. Opanasopit, P. Aumklad, P. Patrojanasophon, Development and evaluation of novel water-based drug-in-adhesive patches for the transdermal delivery of Ketoprofen, Pharmaceutics 13 (2021) 789, https://doi.org/10.3390/pharmaceutics13060789.
[39] J. Fan, T.-D. Lei, J. Li, P.-Y. Zhai, Y.-H. Wang, F.-Y. Cao, Y. Liu, High protein content keratin/poly (ethylene oxide) nanofibers crosslinked in oxygen atmosphere and its cell culture, Mater. Des. 104 (2016) 60–67, https://doi.org/10.1016/j.matdes.2016.05.022.
[40] B. Kalita, M.K. Das, Rutin–phospholipid complex in polymer matrix for long-term delivery of rutin via skin for the treatment of inflammatory diseases, Artif cells Nanomed, Biotechnol 46 (2018) 41–56, https://doi.org/10.1080/21691401.2017.1411931.
[41] M. Schulz, B. Fussnegger, R. Bodmeier, Drug release and adhesive properties of crospovidone-containing matrix patches based on polyisobutene and acrylic adhesives, Eur. J. Pharm. Sci. 41 (2010) 675–684, https://doi.org/10.1016/j.ejps.2010.09.011.
[42] B. Kalita, M.K. Das, Rutin–phospholipid complex in polymer matrix for long-term delivery of rutin via skin for the treatment of inflammatory diseases, Artif cells Nanomed, Biotechnol 46 (2018) 41–56, https://doi.org/10.1080/21691401.2017.1411931.